Emergence of flat bands in the quasicrystal limit of boron nitride twisted bilayers

Lorenzo Sponza, Van Binh Vu, Elisa Serrano Richaud, Hakim Amara, Sylvain Latil

Emergence of flat bands in the quasicrystal limit of boron nitride twisted bilayers

Lorenzo Sponza,[1,2] Van Binh Vu,[3] Elisa Serrano Richaud,[1] Hakim Amara,[1,4] and Sylvain Latil[3]

[1] *Université Paris-Saclay, ONERA, CNRS, Laboratoire d'étude des microstructures (LEM), 92322, Châtillon, France*
[2] *European Theoretical Spectroscopy Facility (ETSF), B-4000 Sart Tilman, Liège, Belgium*
[3] *Université Paris-Saclay, CEA, CNRS, SPEC, 91191 Gif-sur-Yvette, France*
[4] *Université Paris Cité, Laboratoire Matériaux et Phénomènes Quantiques (MPQ), CNRS-UMR7162, 75013 Paris, France*

(Dated: April 2, 2024)

We investigate the electronic structure and the optical absorption onset of close-to-30°twisted hexagonal boron nitride bilayers. Our study is carried out with a purposely developed tight-binding model validated against DFT simulations. We demonstrate that approaching 30°(quasicrystal limit), all bilayers sharing the same moiré supercell develop identical band structures, irrespective of their stacking sequence. This band structure features a bundle of flat bands laying slightly above the bottom conduction state which is responsible for an intense peak at the onset of the absorption spectrum. These results suggest the presence of strong, stable and stacking-independent excitons in boron nitride 30°-twisted bilayers. By carefully analyzing the electronic structure and its spatial distribution, we elucidate the origin of these states as moiré-induced K-valley scattering due to interlayer B−B coupling. We take advantage of the the physical transparency of the tight-binding parameters to derive a simple triangular model based on the B sublattice that accurately describes the emergence of the bundle. Being our conclusions very general, we predict that a similar bundle should emerge in other close-to-30° bilayers, like transition metal dichalcogenides, shedding new light on the unique potential of 2D materials.

The unconventional physical properties exhibited by twisted bilayers have given rise to the field of twistronics.[1–4] By stacking 2D atomic layers, a geometric moiré superlattice emerges as a lattice mismatch and/or a rotational twist.[5] The resulting pattern modulates the potential at the supercell scale and hence changes the electronic band structure typically through the formation of low dispersing bands often presenting peculiar properties.[6–8] Typical examples of moiré composites include the pioneering twisted bilayer graphene,[9] twisted hexagonal boron nitride (hBN)[2,10,11] or hetero- and homobilayers of transition metal dichalcogenides (TMDs).[12] In gapped twisted bilayers, like hBN, the width of band edge states decreases continuously with the angle of twist (no magic angle) and the presence of different atomic species generates several stacking possibilities with specific electronic properties, providing an additional degree of freedom with respect to graphene bilayers.[13–15]

Since the early stages of twistronics, the scientific community has mostly focused on the small twist angle limit. In this context, continuous models[16,17] or tight-binding (TB) hamiltonians[18–21] have been developed and density functional theory (DFT) calculations[17,18] carried out on several 2D material bilayers. Actually, few works treat also larger twisting angles (in the 15°-28°range)[22–24] and even less works consider rotations of 30°[25,26] or very close to it.[18,27] In any case, all these studies focus only on graphene bilayers and mention large angle configurations among other structures, none of them being specifically devoted to the investigation of close-to-30° twists. Regarding hBN, only the 30° twisted bilayers have been considered very recently.[28] DFT calculations suggest that this BN material is a unique wide-gap 2D quasicrystal, yet its electronic and optical properties have never been addressed specifically.

In this Letter, we investigate the band structure and optical response of different stackings of hBN bilayer twisted in the vicinity of 30° using a dedicated TB model. We demonstrate that all structures develop an identical bundle of flat states just above the bottom of the conduction band. We trace its physical origin and develop a simple model describing its formation.

To identify unambiguously the structures, we use the definitions introduced in[15] and recalled in Sec. I of the Supplemental Materials.[29] Our TB model is purposely designed to describe accurately the last occupied and the first empty states Besides permitting calculations in supercells close enough to 30°, the TB formalism also allows to unravel some fundamental mechanism. Our TB model is inspired by literature[18,19,30] and detailed in Sec. II of the Supplemental Materials.[29] A feature it is worth stressing is the distance-dependent exponential decay of the interlayer hopping terms whose prefactor γ^{XY} gives a measure of the interlayer coupling strength, XY labelling the pairings BN, BB and NN. Remarkably, our TB model happens to describe reasonably well the top valence (TV) and bottom conduction (BC) states in a wide range of twist angles, comparing well to other low-angle models.[14,20,31,32]

The quality of the parametrization can be appreciated in Figure 1 where we report the BC and independent-particle (IP) optical spectra computed both with our TB model and ab-initio methods. Ab-initio simulation details are reported in Sec. III of the Supplemental Materials.[29] We present results from the BB(1,3), BN(1,3) and BN(3,8) bilayers, chosen as paradigmatic because of specific characteristics of their band structure, but we checked that the agreement is equally good in the other stackings (cfr. Fig. 6 of Supplemental Materials[29]).

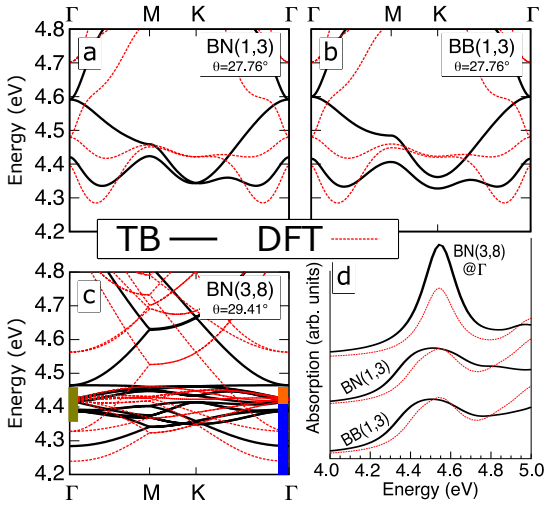

FIG. 1. (a, b, c): Conduction bands of BN(1,3), BB(1,3) and BN(3,8) in TB (black solid) and DFT (red dashed). The TV of all structures have been aligned to 0.0 eV. In (c), tick bars on the canvas highlight notable energy intervals (see text). (d): Onset of IP absorption spectra of the same systems. The BN(3,8) spectra are computed only in the Γ point. All spectra have been broadened with a Lorentzian with variance 0.1 eV.

Our parametrization reproduces the general dispersion of DFT bands and the gapwidth. Particular attention has been paid on the BC. Let us first consider panels (a) and (b), i.e. the two (1,3) supercells. DFT predicts the formation of a pretty flat dispersion in the M-K region in both systems. Actually the two bands avoid each other in the BB(1,3), even though the splitting is extremely small. Instead, they cross at K in the BN(1,3), consistently with what simulated at smaller angles.[15] Our TB model catches very well these features although the splitting in the BB stacking is somewhat overestimated. At a larger angles, like in the BN(3,8), the agreement is even better as panel (c) exemplifies well. In particular, the model predicts correctly the emergence of a group of densely packed and low dispersing bands concentrated between 4.37 eV and 4.46 eV, that we will call the 'bundle' of flat states, highlighted by an olive green side bar in Figure 1c). It is useful to split the conduction bands into a lower energy region (blue bar in Figure 1.c) called 'shallow conduction', and a higher energy region where bands are particularly flat called the 'deep bundle' region (orange bar in Figure 1c). All energy intervals are given with respect to the top of the valence band.

We also evaluated with the two methods the imaginary part of the IP dielectric function[33] $\varepsilon(\omega)$ in the same three systems whose results are reported in panel d of Figure 1. Details on the calculation can be found in Sec. II and III of the Supplemental Materials.[29] Because of the large size of the (3,8) supercell (388 atoms), the ab-initio spectrum is computed only in the Γ point, and the same in TB for sake of comparison. Both methods predict a well-detached peak at 4.5 eV, corresponding to transitions towards the bottom conduction states. Differences between the stackings are negligible, indicating that not only the band structure but also the wavefunctions are remarkably similar in these systems.

Having validated the TB model, we extend our investigation to twist angles closer to 30° and systems hardly attainable with DFT. In panels a to f of Figure 2, we report the BC states of the BB and BN stackings in the (5,13), (4,11) and (11,30) supercells, corresponding to twist angles ranging from 28.78° to 29.96°. The tendency observed already in the (1,3) and (3,8) supercells is here confirmed and strengthened: the stackings present basically the same band structure at fixed supercell. This is actually true for all five stacking, as we assess in Fig. 7 of the Supplemental Materials.[29] The indistinguishability of the stacking sequence when approaching 30° twist comes from the fact that, in this limit, the bilayer approaches a quasicrystal without any translation symmetry. As a consequence, all local configurations are realized somewhere and a sort of self-similarity arise such that in each supercell approximate replicas of smaller cells of all the five stackings can be found. We will encounter another manifestation of this property later on. Actually, the same happens in any homobilayer formed of hexagonal monolayers, so we expect a similar indistinguishability to occur also in close-to-30° twisted graphene, TMDs, silicene and many of the most popular 2D materials.

More interestingly, we observe a bundle of flat states forming in the conduction band of all structures at all angles, comprised in a narrow interval (about 100 meV) centered around 4.40 eV. This is in contrast to small-angle twisted hBN bilayers, where one or more single states are formed directly in the gap and clearly separated in energy by about 0.1 eV.[2,10,13] Because driven by the twist, the corresponding enhancement of the density of states (DOS) is very robust as basically independent on the stacking sequence or on the chemical environment. It is hence deterministic, contrary to a similar enhancement observed in bulk quasicrystals.[34–36]

Our TB formalism allows us to identify easily the origin of the bundle in terms of the monolayer valleys. In fact, since our TB model contain no s orbitals, a Γ component can be excluded from the beginning. A deeper analysis, making use of the unfolding technique[37] and detailed in section IV of the Supplemental Materials,[29] indicates that the bundle comes in fact from states close to the K and M points of the monolayer Brillouin zone. This explains the emergence of similar bundles in graphene-based incommensurate stackings[27,38,39] (even though in these systems they are created symmetrically also in the valence) and suggests that similar bundles should emerge in other hexagonal 2D materials, namely TMDs.

It is particularly worthwhile to study the impact of these flat states on the absorption properties. We used TB to compute the IP optical response in the (5,13) and (4,11) supercells, here reported in Figure 2, panels g and h. As expected, the BN and the BB stackings present very small differences that are further washed out as the twist angle approaches 30°. Spectral onsets are domi-

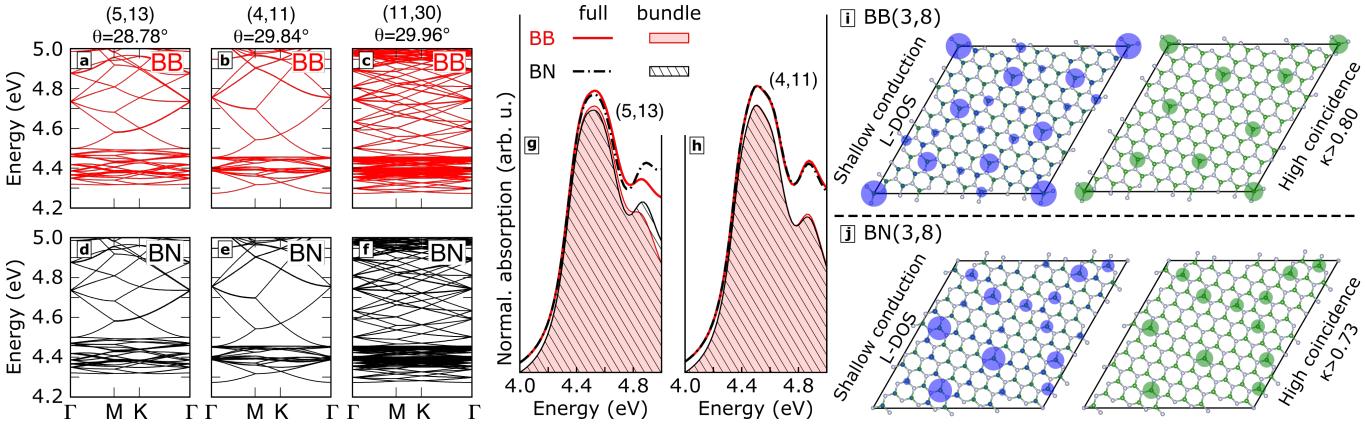

FIG. 2. $(a-c)$: Conduction bands of the BB(5,13), BB(4,11) and BB(11,30) respectively. $(d-f)$: Same as $(a-c)$ in the BN stacking. The TV of all structures have been aligned to 0.0 eV. (g,h): IP absorption spectra of the BB(5,13) and BB(4,11) (red solid curves) and BN(5,13) and BN(4,11) (black dashed) obtained including all empty and occupied states (full). Shaded and patterned areas are obtained by restricting the empty states between 4.34 eV and 4.48 eV. (i,j): Blue circles: Radius proportional to the L-DOS in the shallow conduction interval. Green circles: Radius proportional to $\mathcal{C}_{j_B}(\mathbf{d})$ wherever it is higher than κ. See main text for details. Data are shown only for the upper layers of the BB(3,8) (i) and BN(3,8) systems (j).

nated by the same intense and well detached peak observed in Figure 1.d). Spectra including only transitions toward the bundle (4.34 eV to 4.48 eV) recover essentially the same signal. This demonstrates that quasicrystallinity has a strong impact on the smallest excitations of this material because the bundle, despite not being the BC, is solely responsible of the absorption onset. In this respect, BN-based quasicrystals are very different from graphene ones[27,38,39] where the low-energy physics is still dominated by monolayer-like Dirac cones. Given these results, we predict that close-to-30° twisted hBN bilayers will display exceptionally strong, robust (and possibly localised) electron-hole excitations.

To go beyond in the analysis, we look at the spatial distribution of the conduction states by evaluating the local DOS (L-DOS) in energy intervals corresponding to the deep bundle and the shallow conduction highlighted in Figure 1.c). We show results in the upper layer of the (3,8) supercells, because pictures are easier to read than in larger structures. In Figure 2, the radius of the blue circles in panels i and j is proportional to the L-DOS in the upper layer of the BB(3,8) and BN(3,8) respectively. No DOS is centered on N sites since they contribute only to valence states.[40] Despite the resemblance of both band structures and optical spectra, the two stacking develop quite different patterns which actually hide fascinating similarities. In fact inside each structure, one can find infinite rearrangements of smaller-cell approximants of all the five stackings repeating themselves in a kind of self-similar scheme. The L-DOS patterns of Figure 2 arise from a sort of frustrated interference between these lower order configurations. Examples of this are presented in Sec. VII of the Supplemental Materials,[29] but further studies go beyond the scope of this article. The L-DOS appears to be stronger on sites where B atoms of the two layers are almost vertically aligned. To highlight better this feature, we evaluate at each B site j_B the coincidence function $\mathcal{C}_{j_B}(\mathbf{d}) = 1 - d_{xy}/D$, where d_{xy} is the in-plane component of the vector $\mathbf{d}$ connecting the site j_B of one layer to the closest B site of the other layer and $D = 1.452$ Å is the in-plane interatomic distance. By definition, $\mathcal{C}_{j_B}(\mathbf{d}) = 1$ if two j_B and a B atom of the other layer are vertically aligned, and decreases linearly to 0 where j_B is aligned with a N or a hexagon center. The radius of green circles of Figure 2 i and j, is proportional to $\mathcal{C}_{j_B}(\mathbf{d})$ of all B sites of the upper layer for which $\mathcal{C}_{j_B}(\mathbf{d}) > \kappa$ where $\kappa = 0.8$ in BB(3,8) and $\kappa = 0.73$ in BN(3,8). The resemblance between the high-coincidence patterns and the shallow conduction L-DOS is striking. The same can be shown for the "deep bundle" states and low coincidence patterns (cfr. Fig. 5 of the Supplemental Materials). This analysis reveals that B−B interlayer states play a crucial role in the bundle formation and that the more vertical the B−B alignment, the stronger the coupling and hence the lower the energy of the corresponding empty state. These are actually bonding states because the TB coefficients of coinciding and quasi-coinciding sites change sign in the two layers.

Inspired by this analysis, we calculate the band structure of the BN(3,8) including all TB parameters except for the prefactor of the B−B interlayer coupling γ^{BB} which we set to zero. The resulting states are reported in Figure 3 a). They are dispersing and are basically indistinguishable from those of a monolayer. If we now set $\gamma^{BB} = 1.225$ eV (50%) (panel b), then localized states begin forming until a bundle of completely flat bands emerges at $\gamma^{BB} = 2.45$ eV (100%) in panel c. The weakness of the interlayer N−N coupling explains why there is no such a feature in the valence band, contrary to what happens in graphene twisted bilayers where conduction-conduction and valence-valence couplings are equivalent.[41]

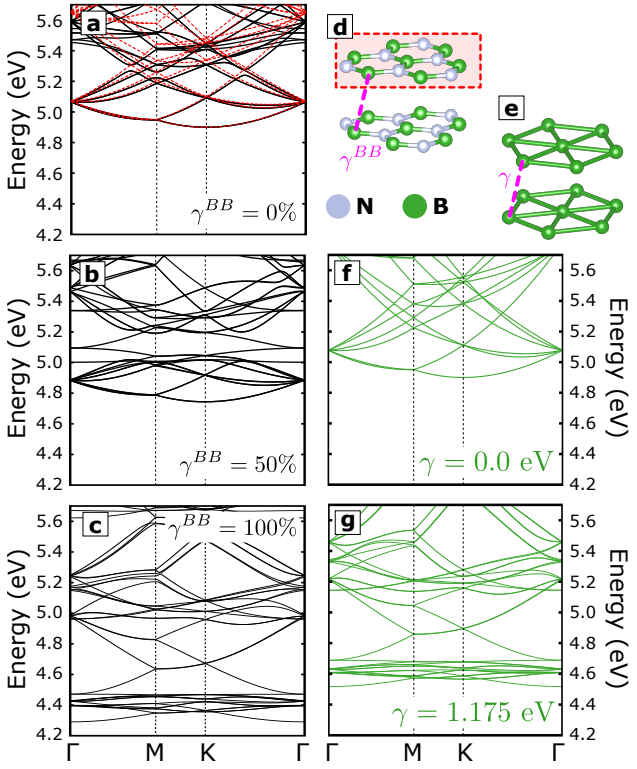

FIG. 3. (a): TB conduction band of the monolayer in the (3,8) supercell (dashed red) and of the BB(3,8) with $\gamma^{BB} = 0$ eV. (b and c): The same bilayer with γ^{BB} equal to 50% and 100% of the correct value. The top valence of all structures have been aligned to 0.0 eV. (d): Ball and stick model of the actual twisted bilayer. Dashed magenta line: the γ^{BB} interlayer coupling. Red shaded area: the isolated monolayer. (e) Ball and stick model of the triangular lattice twisted bilayer made only of B sites. Dashed magenta line: the γ interlayer coupling. (f and g): bands of the triangular model with γ= 0 eV and 1.715 eV respectively.

We then devise an even simpler TB model which describes the formation of the bundle states. We select only the B sublattices obtaining a structure formed of two triangular lattice where only B−B interactions are taken into account. Details of the model and its relation to the full honeycomb model are reported in Sec. V of the Supplemental Materials.[29] The conduction band structure of this simplified triangular model is reported in Figures 3 f and g respectively for vanishing and non-vanishing interlayer coupling. The model reproduces the isolated honeycomb monolayer at no coupling and gives rise to a bundle of flat bands at full coupling remarkably similar to the honeycomb TB model, clearly demonstrating that B−B interlayer interaction is solely responsible of the localization of the electrons in high-angle twisted BN bilayers. This model allows us to unravel a fundamental mechanism common to other large-angle twisted bilayers. We deem probable that a similar bundle of flat states will emerge in the valence band of close-to-30° twisted TMDs where the interlayer coupling is mostly due to chalcogen p_z states which form the top of the valence band.[17]

To conclude, we have investigated the electronic and optical properties of hBN bilayers at twist angles close to 30° by means of a purposely developed TB model. We have demonstrated that in this range of angles all hBN bilayers develop the same electronic properties, irrespective of the stacking sequence. This is characterised by the emergence of a bundle of low-dispersing states right above the bottom of the conduction band. This results from a strong coupling between B atoms belonging to different layers and is responsible of an intense and robust peak at the onset of the absorption spectrum. The asymmetry of the corresponding DOS enhancement and its dominant role in the absorption onset, make hBN quasicrystals very different from the other 2D quasicrystals studied so far (mainly 30°-twisted graphene bilayer,[27,38] and incommensurate stacks of graphene trilayers.[39] We captured this fundamental mechanism with a very simple triangular lattice TB model which can be applied to many other twisted bilayers (e.g. homobilayers of TMDs). Our results suggest that 30°-twisted BN bilayers may host extremely strong excitonic phenomena originated by the bundle of flat bands and independent on the stacking sequence. Owing to its geometrical origin, similar bundles are expected to emerge in the valence band of TMDs quasicrystals, probaly with similar consequences on their excitonic properties. Moreover, its robustness with respect to the stacking sequence is expected to be an ubiquitous characteristic in the quasicrystal limit, and to occur in twisted bilayers of other 2D materials including TMDs, antimonene, silicene, transition metal monochalcogenides, and all homostructures formed of hexagonal single-layers.

ACKNOWLEDGMENTS

The authors acknowledge funding from the European Union's Horizon 2020 research and innovation program under grand agreement No◦ 881603 (Graphene Flagship core 3) and from public grants overseen by the French National Research Agency (ANR) as part of the 'Investissements d'Avenir' program (Labex NanoSaclay, reference: ANR-10-LABX-0035) and under the EXCIPLINT project (Grant No. ANR-21-CE09-0016).

[1] S. Carr, S. Fang, and E. Kaxiras, "Electronic-structure methods for twisted moiré layers," Nat. Rev. Mater. **5**, 748–763 (2020).

[2] B. Liu, L. Xian, H. Mu, G. Zhao, Z. Liu, A. Rubio, and Z. F. Wang, "Higher-Order Band Topology in Twisted Moiré Superlattice," Phys. Rev. Lett. **126**, 066401 (2021).

[3] E. Y. Andrei, D. K. Efetov, P. Jarillo-Herrero, A. H. MacDonald, K. F. Mak, T. Senthil, E. Tutuc, A. Yazdani, and A. F. Young, "The marvels of moiré materials," Nat. Rev. Mater. **6**, 201–206 (2021).

[4] L. Du, M. R. Molas, Z. Huang, G. Zhang, F. Wang, and Z. Sun, "Moiré photonics and optoelectronics," Science **379**, eadg0014 (2023).

[5] D. Gratias and M. Quiquandon, "Crystallography of homophase twisted bilayers: coincidence, union lattices and space groups," Acta Cryst. **A79**, 301–317 (2023).

[6] M. Yankowitz, S. Chen, H. Polshyn, Y. Zhang, K. Watanabe, T. Taniguchi, D. Graf, A. F. Young, and C. R. Dean, "Tuning superconductivity in twisted bilayer graphene," Science **363**, 1059–1064 (2019).

[7] L. Balents, C. R. Dean, D. K. Efetov, and A. F. Young, "Superconductivity and strong correlations in moiré flat bands," Nat. Phys. **16**, 725–733 (2020).

[8] Y. Cao, V. Fatemi, A. Demir, S. Fang, S. L. Tomarken, Jason Y. Luo, J. D. Sanchez-Yamagishi, K. Watanabe, T. Taniguchi, E. Kaxiras, R. C. Ashoori, and P. Jarillo-Herrero, "Correlated insulator behaviour at half-filling in magic-angle graphene superlattices," Nature **556**, 80–84 (2018).

[9] R. Bistritzer and A. H. MacDonald, "Moiré bands in twisted double-layer graphene," Proc. Natl. Acad. Sci. USA **108**, 12233–12237 (2011).

[10] L. Xian, D. M. Kennes, N. Tancogne-Dejean, M. Altarelli, and A. Rubio, "Multiflat Bands and Strong Correlations in Twisted Bilayer Boron Nitride: Doping-Induced Correlated Insulator and Superconductor," Nano Lett. **19**, 4934 (2019).

[11] D. S. Kim, R. C. Dominguez, R. Mayorga-luna, D. Ye, J. Embley, T. Tan, Y. Ni, Z. Liu, M. Ford, F. Y. Gao, S. Arash, K. Watanabe, T. Taniguchi, S. Kim, C.-K. Shih, K. Lai, W. Yao, L. Yang, X. Li, and Y. Miyahara, "Electrostatic moiré potential from twisted hexagonal boron nitride layers," Nat Mater. (2023), 10.1038/s41563-023-01637-7.

[12] G. Scuri, T. I. Andersen, Y. Zhou, D. S. Wild, J. Sung, R. J. Gelly, D. Bérubé, H. Heo, L. Shao, A. Y. Joe, A. M. Mier Valdivia, T. Taniguchi, K. Watanabe, M. Lončar, P. Kim, M. D. Lukin, and H. Park, "Electrically tunable valley dynamics in twisted WSe_2/WSe_2 bilayers," Phys. Rev. Lett. **124**, 217403 (2020).

[13] X.-J. Zhao, Y. Yang, D.-B. Zhang, and S.-H. Wei, "Formation of bloch flat bands in polar twisted bilayers without magic angles," Phys. Rev. Lett. **124**, 086401 (2020).

[14] N. R. Walet and F. Guinea, "Flat bands, strains, and charge distribution in twisted bilayer h-BN," Phys. Rev. B **103**, 125427 (2021).

[15] S. Latil, H. Amara, and L. Sponza, "Structural classification of boron nitride twisted bilayers and ab initio investigation of their stacking-dependent electronic structure," SciPost Phys. **14**, 053 (2023).

[16] M. G. Scheer, K. Gu, and B. Lian, "Magic angles in twisted bilayer graphene near commensuration: Towards a hypermagic regime," Phys. Rev. B **106**, 115418 (2022).

[17] S. Fang, R. K. Defo, S. N. Shirodkar, S. Lieu, G. A. Tritsaris, and E. Kaxiras, "Ab initio tight-binding hamiltonian for transition metal dichalcogenides," Phys. Rev. B **92**, 205108 (2015).

[18] G. Trambly de Laissardière, D. Mayou, and L. Magaud, "Localization of Dirac electrons in rotated graphene bilayers," Nano Lett. **10**, 804–808 (2010).

[19] S. Venkateswarlu, A. Honecker, and G. Trambly de Laissardière, "Electronic localization in twisted bilayer MoS_2 with small rotation angle," Phys. Rev. B **102**, 081103 (2020).

[20] M. Long, P. A. Pantaleón, Z. Zhan, F. Guinea, J. A. Silva-Guillén, and S. Yuan, "An atomistic approach for the structural and electronic properties of twisted bilayer graphene-boron nitride heterostructures," npj Comput. Mater. **8**, 73 (2022).

[21] H. Ochoa and A. Asenjo-Garcia, "Flat Bands and Chiral Optical Response of Moiré Insulators," Phys. Rev. Lett. **125**, 37402 (2020), arXiv:2002.09804.

[22] A. O. Sboychakov, A. L. Rakhmanov, A. V. Rozhkov, and Franco Nori, "Electronic spectrum of twisted bilayer graphene," Phys. Rev. B **92**, 075402 (2015).

[23] H. K. Pal, S. Spitz, and M. Kindermann, "Emergent geometric frustration and flat band in moiré bilayer graphene," Phys. Rev. Lett. **123**, 186402 (2019).

[24] C. Mondal, R. Ghadimi, and B.-J. Yang, "Quantum valley and subvalley hall effect in large-angle twisted bilayer graphene," Phys. Rev. B **108**, L121405 (2023).

[25] S. J. Ahn, P. Moon, T.-H. Kim, H.-W. Kim, H.-C. Shin, E. H. Kim, H. W. Cha, S.-J. Kahng, P. Kim, M. Koshino, Y.-W. Son, C.-W. Yang, and J. R. Ahn, "Dirac electrons in a dodecagonal graphene quasicrystal," Science **361**, 782–786 (2018).

[26] W. Yao, E. Wang, C. Bao, Y. Zhang, K. Zhang, K. Bao, C. K. Chan, C. Chen, J. Avila, M. C. Asensio, J. Zhu, and S. Zhou, "Quasicrystalline 30° twisted bilayer graphene as an incommensurate superlattice with strong interlayer coupling," Proc. Natl. Acad. Sci. USA **115**, 6928–6933 (2018).

[27] P. Moon, M. Koshino, and Y.-W. Son, "Quasicrystalline electronic states in 30° rotated twisted bilayer graphene," Phys. Rev. B **99**, 165430 (2019).

[28] L. A. Chernozatonskii and A. I. Kochaev, "BN Diamane-like Quasicrystal Based on 30° Twisted h-BN Bilayers and Its Approximants: Features of the Atomic Structure and Electronic Properties," Crystals **13**, 421 (2023).

[29] See Supplemental Material [url] for details on the nomenclature defining the structures, on the DFT calculation parameters and software,[42–47] on the tight-binding models and for complementary results and analysis.

[30] G. Trambly de Laissardière, D. Mayou, and L. Magaud, "Numerical studies of confined states in rotated bilayers of graphene," Phys. Rev. B **86**, 125413 (2012).

[31] J. C. G. Henriques, B. Amorim, R. M. Ribeiro, and N. M. R. Peres, "Excitonic response of AA' and AB stacked hbn bilayers," Phys. Rev. B **105**, 115421 (2022).

[32] P. Roman-Taboada, E. Obregon-Castillo, A. R. Botello-Mendez, and C. Noguez, "Excitons in twisted AA' hexagonal boron nitride bilayers," Phys. Rev. B **108**, 075109 (2023).

[33] G. Grosso and G. P. Parravicini, "Chapter 12 - Optical Properties of Semiconductors and Insulators," in *Solid State Physics (Second Edition)*, edited by G. Grosso and G. P. Parravicini (Academic Press) pp. 529–576.

[34] T. Fujiwara, "Electronic structure in three-dimensional quasicrystals," J. Non-Cryst. Solids **117-118**, 844–847 (1990).

[35] S. Roche, G. Trambly de Laissardière, and D. Mayou, "Electronic transport properties of quasicrystals," J. Math. Phys. **38**, 1794–1822 (1997), https://pubs.aip.org/aip/jmp/article-pdf/38/4/1794/19255683/1794_1_online.pdf.

[36] M. Krajcí and J. Hafner, "Fermi surfaces and electronic transport properties of quasicrystalline approximants," Journal of Physics: Condensed Matter **13**, 3817 (2001).
[37] P. B. Allen, T. Berlijn, D. A. Casavant, and J. M. Soler, "Recovering hidden bloch character: Unfolding electrons, phonons, and slabs," Phys. Rev. B **87**, 085322 (2013).
[38] Guodong Yu, Zewen Wu, Zhen Zhan, Mikhail I. Katsnelson, and Shengjun Yuan, "Dodecagonal bilayer graphene quasicrystal and its approximants," npj Computational Materials **5**, 122 (2019), arXiv:1907.08792.
[39] A. Uri, S. C. de la Barrera, M. T. Randeria, D. Rodan-Legrain, T. Devakul, P. J. D. Crowley, N. Paul, K. Watanabe, T. Taniguchi, R. Lifshitz, L. Fu, R. C. Ashoori, and P. Jarillo-Herrero, "Superconductivity and strong interactions in a tunable moiré quasicrystal," Nature **620**, 762–767 (2023).
[40] T. Galvani, F. Paleari, H. Miranda, A. Molina-Sánchez, L. Wirtz, S. Latil, H. Amara, and F Ducastelle, "Excitons in boron nitride single layer," Phys. Rev. B **94**, 125303 (2016).
[41] G. Yu, Y. Wang, M. I. Katsnelson, and S. Yuan, "Origin of the magic angle in twisted bilayer graphene from hybridization of valence and conduction bands," Phys. Rev. B **108**, 045138 (2023).
[42] P. Giannozzi, S. Baroni, N. Bonini, M. Calandra, R. Car, C. Cavazzoni, D. Ceresoli, G. L. Chiarotti, M. Cococcioni, I. Dabo, A. Dal Corso, S. de Gironcoli, S. Fabris, G. Fratesi, R. Gebauer, U. Gerstmann, C. Gougoussis, A. Kokalj, M. Lazzeri, L. Martin-Samos, N. Marzari, F. Mauri, R. Mazzarello, S. Paolini, A. Pasquarello, L. Paulatto, C. Sbraccia, S. Scandolo, G. Sclauzero, A. P. Seitsonen, A. Smogunov, P. Umari, and R. M. Wentzcovitch, "QUANTUM ESPRESSO: a modular and open-source software project for quantum simulations of materials," J. Phys.: Condens. Matter **21**, 395502 (2009).
[43] P. Giannozzi, O. Andreussi, T. Brumme, O. Bunau, M. Buongiorno Nardelli, M. Calandra, R. Car, C. Cavazzoni, D. Ceresoli, M. Cococcioni, N. Colonna, I. Carnimeo, A. Dal Corso, S. de Gironcoli, P. Delugas, R. A. DiStasio, A. Ferretti, A. Floris, G. Fratesi, G. Fugallo, R. Gebauer, U. Gerstmann, F. Giustino, T. Gorni, J. Jia, M. Kawamura, H.-Y. Ko, A. Kokalj, E. Küçükbenli, M. Lazzeri, M. Marsili, N. Marzari, F. Mauri, N. L. Nguyen, H.-V. Nguyen, A. Otero de-la Roza, L. Paulatto, S. Poncé, D. Rocca, R. Sabatini, B. Santra, M. Schlipf, A. P. Seitsonen, A. Smogunov, I. Timrov, T. Thonhauser, P. Umari, N. Vast, X. Wu, and S. Baroni, "Advanced capabilities for materials modelling with QUANTUM ESPRESSO," J. Phys.: Condens. Matter **29**, 465901 (2017).
[44] J. D. Pack and H. J. Monkhorst, "special points for Brillouin-zone integrations"-a reply," Phys. Rev. B **16**, 1748–1749 (1977).
[45] J. P. Perdew, K. Burke, and M. Ernzerhof, "Generalized gradient approximation made simple," Phys. Rev. Lett. **77**, 3865–3868 (1996).
[46] A. Marini, C. Hogan, M. Grüning, and D. Varsano, "yambo: An ab initio tool for excited state calculations," Comput. Phys. Commun. **180**, 1392–1403 (2009).
[47] D. Sangalli, A. Ferretti, H. Miranda, C. Attaccalite, I. Marri, E. Cannuccia, P. Melo, M. Marsili, F. Paleari, A. Marrazzo, G. Prandini, P. Bonfà, M. O. Atambo, F. Affinito, M. Palummo, A. Molina-Sánchez, C. Hogan, M. Grüning, D. Varsano, and A. Marini, "Many-body perturbation theory calculations using the yambo code," J. Phys.: Condens. Matter **31**, 325902 (2019).